



Cite this: DOI: 10.1039/c7dt01323j

Four-component zinc-porphyrin/zinc-salphen nanorotor†

Merve S. Özer, Anup Rana, Pronay K. Biswas and Michael Schmittel *

An off-axis supramolecular rotor was composed of four components: a zinc-porphyrin based stator with four phenanthroline stations and a zinc-salphen based rotator were self-assembled with DABCO and four copper(I) ions to furnish the rotor **ROT-2** in quantitative yield. The DABCO serves as a connecting axle between the rotator and the stator, while the rotator is additionally connected to two copper(I)-loaded phenanthroline stations of the stator *via* its two pyridine terminals ($N_{py} \rightarrow [Cu(phen)]^+$). For the thermally activated rotation both $N_{py} \rightarrow [Cu(phen)]^+$ interactions have to be cleaved. Due to the high energy barrier of the rotation the slow motion was monitored by ROESY. The reduced speed ($k_{298} = 0.2 \text{ s}^{-1}$) was rationalised in terms of ground state stabilisation of the rotor as suggested by computational insight. Additional VT $^1\text{H-NMR}$ investigation was undertaken to study the motion of DABCO that is sandwiched between zinc porphyrin and zinc salphen. The diagnostic splitting of the geminal DABCO protons was rationalised on the basis of the asymmetry induced by the salphen that generates a diastereotopic environment. Computations reproduced the experimental NMR with excellent agreement.

Received 12th April 2017,
Accepted 23rd June 2017

DOI: 10.1039/c7dt01323j

rsc.li/dalton

Introduction

Inspired by nature, useful and fascinating molecular machines^{1–3} – mostly based on covalent frameworks – have been constructed for highly specific tasks and practical work.⁴ New design principles⁵ allowing multi-component assembly^{6–10} in combination with well-established thermally activated motion, such as translation^{11,12} and rotation,¹³ should open the door for creating new multi-component machinery with interesting dynamic behavior.^{14–17} Recently, various multicomponent nanorotors were prepared by our group.¹⁸ In the four-component nanorotors,^{18a} two distinctly ornamented zinc porphyrins (stator and rotator) are sandwiched together by means of two axial $N_{DABCO} \rightarrow \text{zinc(II)}$ porphyrin (ZnPor) and two $N_{py} \rightarrow [Cu(phen)]^+$ interactions (= HETPYP binding: HETeroleptic PYridine and Phenanthroline metal complexation¹⁹), a building principle that we will also apply in the actual investigation.

Here, we present a four-component off-axis nanorotor. Different from previous work, the porphyrin unit of the rotator is replaced by a salphen core and the DABCO axle connects with the rotator off the midpoint between the two pyridine terminals.²⁰ The salphen moiety has found ample use as a building

block in materials chemistry applications,²¹ suggesting its valuable utility in supramolecular machinery as well.

Results and discussion

For the off-axis supramolecular rotor, we chose zinc porphyrin-based stator **1** and zinc-salphen skeleton **2** as a rotator (Chart 1), the latter equipped with *tert*-butyl groups to overcome solubility problems.²²

The synthetic scheme leading to zinc salphen **2** is illustrated in Scheme 1. Compounds **5**,²³ **6**,²⁴ **7**²⁵ and **8**²⁶ were prepared according to the literature procedures. Two subsequent Suzuki couplings afforded the pyridine-terminated salicylaldehyde **10** in good yield from compounds **7** and **8**. Finally, the condensation of salicylaldehyde **10** and the *ortho*-phenylene diamine derivative **11** in the presence of $Zn(OAc)_2$ afforded the desired zinc salphen **2** in good yield (86%). A full characterisation of rotator **2** was possible by NMR, ESI-MS and elemental analysis. The NMR spectra had to be recorded in $DMSO-d_6$ as a coordinating solvent to prevent the de-metallation of the salphen ligand.²⁷ In DCM, rotator **2** experienced de-metallation as confirmed by ESI-MS (Fig. S15†), whereas the desired peak $m/z = 937.7$ was observed in THF (Fig. S16†).

Analogous to the procedure leading to the known rotor^{18a} $[Cu_2(\mathbf{1})(\mathbf{3})(DABCO)]^{2+}$, we combined compounds **1** and **2** with DABCO and copper(I) ions (1:1:1:2) affording the four-component rotor **ROT-1** = $[Cu_2(\mathbf{1})(\mathbf{2})(DABCO)]^{2+}$ (Scheme 2). $^1\text{H NMR}$ confirmed the formation of the rotor assembly, in

Center for Micro- and Nanochemistry and Engineering, Organische Chemie I, Universität Siegen, D-57068 Siegen, Germany.

E-mail: schmittel@chemie.uni-siegen.de

† Electronic supplementary information (ESI) available. See DOI: 10.1039/c7dt01323j

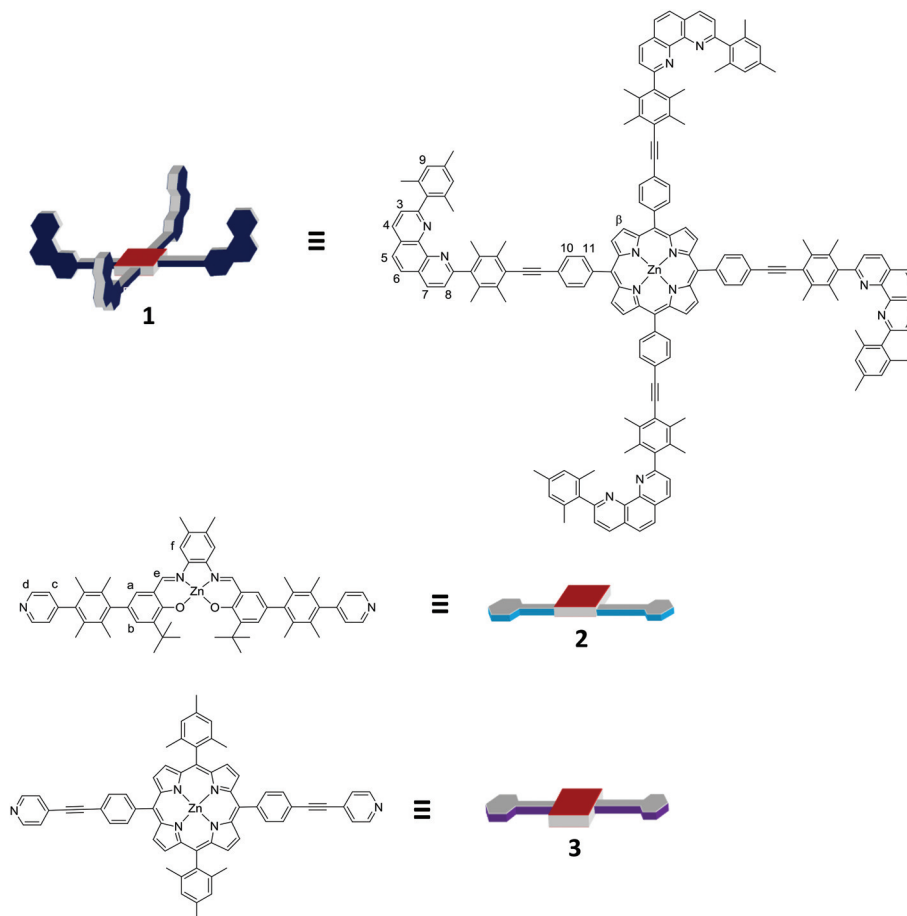
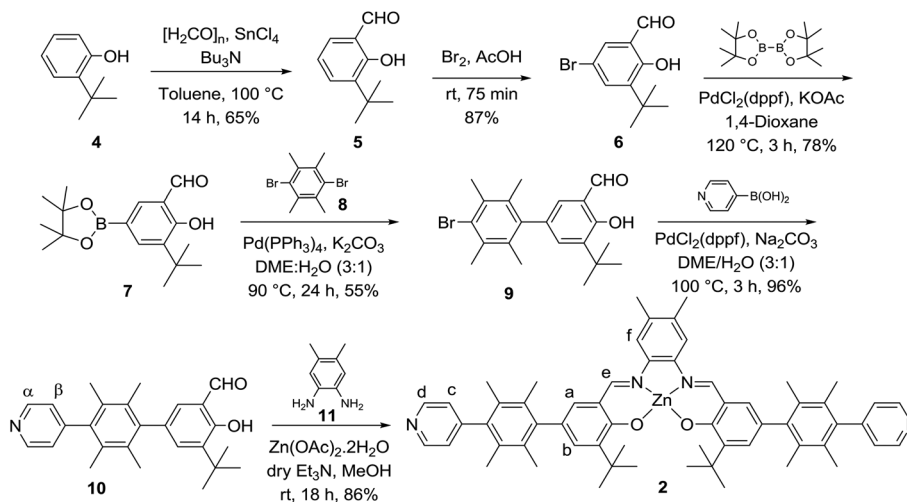


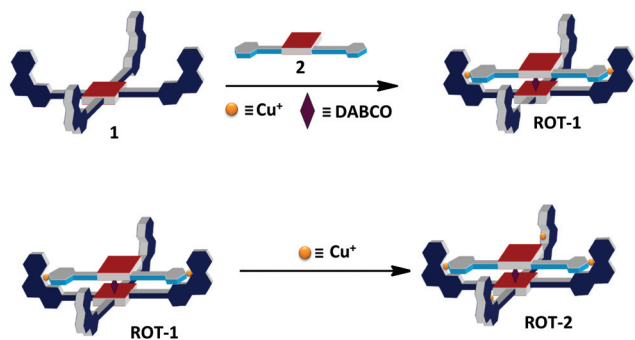
Chart 1 Molecular structures and cartoon representations of stator **1** and rotator **2** & **3** units.



Scheme 1 Synthetic scheme leading to rotator **2**.

particular by comparison with the earlier reported NMR data.^{18a} For instance, ¹H NMR shows the pyridine protons c-H and d-H to be characteristically upfield shifted at 7.01 and 6.92 ppm, respectively. It suggests that the 5,15-positions of

the stator are connected to the rotators' pyridine terminals *via* two $\text{N}_{\text{py}} \rightarrow [\text{Cu}(\text{phen})]^+$ (= HETPYP) interactions (Fig. S7†). Furthermore, the diagnostic signals resonating at 0.47 and -3.10 ppm indicate that DABCO is sandwiched between the



Scheme 2 Preparation of ROT-1 and ROT-2 (cartoon representation).

stator and the rotator, which was also proven by a correlation in the ^1H - ^1H COSY spectrum (Fig. S8†). In contrast to the zinc porphyrin with its strong ring current causing upfield shifts ($\delta_{\text{DABCO}} = -3.10$ ppm),²⁸ the salphen does not instigate drastic changes upon axial coordination.^{20a} Therefore, the chemical shifts of the DABCO protons differ drastically. Furthermore, the proton signals of the four phenanthroline stations in stator **1** appear as two sets, one for the phenanthrolines loaded with the rotator and Cu^+ , and the other for the unloaded free stations.

In spite of DABCO being sandwiched between the rotator and the stator as clearly evidenced by the characteristic signals in ^1H NMR, the ESI-MS was devoid of a mass peak proving the presence of $[\text{Cu}_2(\mathbf{1})(2)(\text{DABCO})]^{2+}$ for ROT-1 possibly due to the lower binding constant of DABCO to $\text{Zn}^{\text{II}}(\text{salphen})$.^{20b} In fact, the ESI-MS reveals a mass peak at 1777.3 representing the assembly $[\text{Cu}_2(\mathbf{1})(2)]^{2+}$ without DABCO (Fig. S17 and S18†). Equally, DABCO was not detected in the other mass peaks appearing in the mass spectrum.

Due to the symmetry of the rotor, the rotation in ROT-1 cannot be investigated by ^1H NMR. Thus, two more equivalents of $[\text{Cu}(\text{CH}_3\text{CN})_4]\text{PF}_6$ were added to ROT-1 to furnish rotor ROT-2 (Scheme 2). Originally, it was assumed that all four stations of the stator would be equivalent in ^1H NMR due to the rapid rotation, but still two sets of phenanthroline protons were detected in ROT-2. Diagnostically, the protons of the previously “free” stations were shifted downfield due to the complexation by Cu^+ ions, as outlined in Fig. 1. The individual chemical shift differences between the two sets of phenanthrolines amount to 0.24–0.38 ppm (Table S1†). In the case of ROT-2, there appears an additional signal belonging to DABCO at 0.11 ppm (for explanation, *vide infra*) apart from the two signals at 0.47 and -3.10 ppm. The DOSY spectrum indicates that there is a single diffusion coefficient at $D = 3.2 \times 10^{-10} \text{ m}^2 \text{ s}^{-1}$ belonging to the assembly including DABCO and its hydrodynamic radius was calculated as 17 Å (Fig. S11†).

Clearly, finding two sets of phenanthrolines in ROT-2 suggests that the rotation is slower than the NMR time scale. For slower exchange processes in dynamic systems 2D NMR techniques, such as EXSY²⁹ or ROESY, may be useful. For ROT-2, the use of the ROESY method³⁰ provided the rate con-

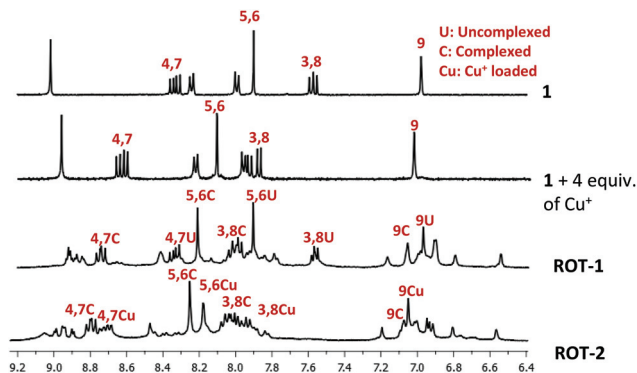


Fig. 1 Partial ^1H NMR spectra of stator **1**, the copper(i)-loaded stator $[\text{Cu}_4(\mathbf{1})]^{4+}$ (1 + 4 equiv. of Cu^+), ROT-1 and ROT-2 in CD_2Cl_2 .

stant $k_{298} = 0.2 \text{ s}^{-1}$ (Fig. S12 and S13†) from the integration of the diagonal and cross signals. As a result, the energy barrier of rotational spinning was determined as $\Delta G_{298}^\ddagger = 77.0 \text{ kJ mol}^{-1}$.

To rationalise the high rotational barrier for rotor ROT-2, we undertook computations and started with a comparison of the ground state stabilisation of ROT-2 vs. ROT-3 = $[\text{Cu}_4(\mathbf{1})(3)(\text{DABCO})]^{4+}$, the latter representing a high-speed rotor ($\Delta G_{298}^\ddagger = 45.0 \text{ kJ mol}^{-1}$).^{18a} For fast computations, two model systems, ROT-2' & ROT-3', were constructed from ROT-2 and ROT-3; a representative of ROT-2' is illustrated in Fig. 2. In both model systems, the two stator arms which are not coordinated *via* copper(i) ions to the pyridines of the rotator are omitted. The model systems as well as both rotators 2 and 3 were optimised by applying the ONIOM method as implemented in Gaussian 09.³¹ The low layer was treated with PM6-D3 and the high layer with DFT-D3.³² Finally, the isodesmic reaction shown in Scheme 3 was evaluated computationally revealing that rotor ROT-2' is more stable than ROT-3' by 33.9 kJ mol^{-1} . A substantial portion of the energy difference, *i.e.* 13.8 kJ mol^{-1} , arises from dispersion. Interestingly, the experimental $\Delta\Delta G_{298}^\ddagger = 32.0 \text{ kJ mol}^{-1}$ between the two rotors ROT-2 and ROT-3 matches well with the computed difference in the ground-state energy of 33.9 kJ mol^{-1} . Such a finding indicates that the rotators' pyridine terminals of both rotors ROT-2 and ROT-3 have almost fully dissociated from their copper(i) centres in the transition state, because only in a late transition state we expect the ground state difference to correspond to

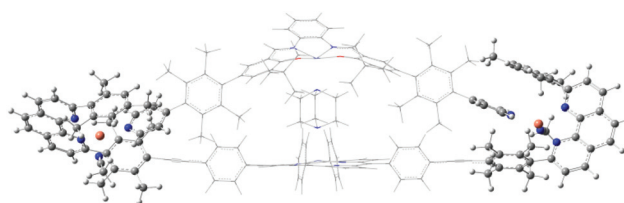
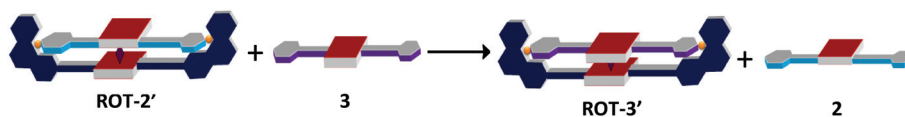


Fig. 2 ONIOM partition for the model system ROT-2' (see Scheme 3). The ball & stick model is for the high layer and the wireframe is for the low layer.



Scheme 3 Isodesmic reaction to check the relative ground state stability of ROT-2' and ROT-3'.

the transition state difference. Moreover this result suggests that even though the local environment of the $N_{\text{py}} \rightarrow [\text{Cu}(\text{phen})]^+$ interactions is identical in both rotors, a large difference may arise due to the strain in the bent assembly and dispersion effects between the rotator and the stator.

In order to confirm the presence of DABCO within the assembly, a VT ^1H NMR of ROT-2 was recorded (Fig. 3a). Despite the fast rotation of DABCO at room temperature,³³ the six protons next to the salphen unit are not equivalent and they resonate as two broad signals with the ratio 1 : 1. Upon cooling down to $-75\text{ }^\circ\text{C}$, the chemical shift difference between the magnetically non-equivalent protons increased, yet at the same time the six DABCO protons next to the porphyrin equally started splitting (ratio 1 : 1).

This phenomenon was further investigated by computational studies. To obtain a reasonably good geometry mimicking the real porphyrin–DABCO–salphen sandwich complex, a different partition scheme (Fig. 4) was applied for the ONIOM computations. Now, the porphyrin–DABCO–salphen sandwich was treated in the high layer by applying the DFT³⁴ method while the rest of ROT-2' was evaluated on the PM6-D3 level. Then, for a conformational analysis the sandwiched DABCO was rotated about the $\text{Zn}-N_{\text{DABCO}}-N_{\text{DABCO}}-\text{Zn}$ axis. Two minima were located, denoted as **conf-1** and **conf-2** in Fig. 5. Their relative populations change from 1.00 over 0.25 ($25\text{ }^\circ\text{C}$) to 0.29 ($0\text{ }^\circ\text{C}$), 0.34 ($-25\text{ }^\circ\text{C}$), 0.42 ($-50\text{ }^\circ\text{C}$) and 0.54 ($-75\text{ }^\circ\text{C}$).

Finally to compute the NMR³⁵ spectra, two simplified model systems, **Conf-1_M** and **Conf-2_M** (Fig. 6), were constructed to mimic **Conf-1** and **Conf-2** (for justification, see the ESI†). Because the rotation of DABCO is too fast to be frozen in our VT experiments (the overall rotational barrier is computed as 8.4 kJ mol^{-1} at $25\text{ }^\circ\text{C}$), the computed chemical shifts for H^1 ,

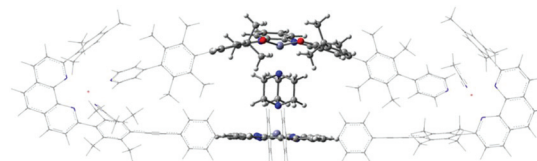


Fig. 4 ONIOM partition of ROT-2' for NMR computations. The ball & stick model is for the high layer and the wireframe is for the low layer.

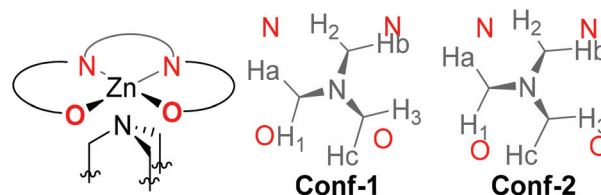


Fig. 5 Schematic representation of the two minima **Conf-1** and **Conf-2**. Red atoms represent those from zinc salphen.

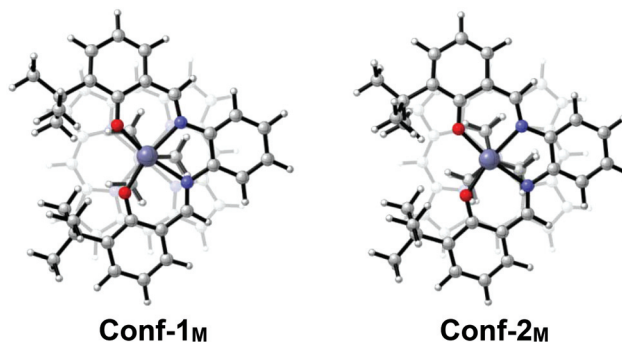


Fig. 6 **Conf-1_M** and **Conf-2_M** for NMR computation.

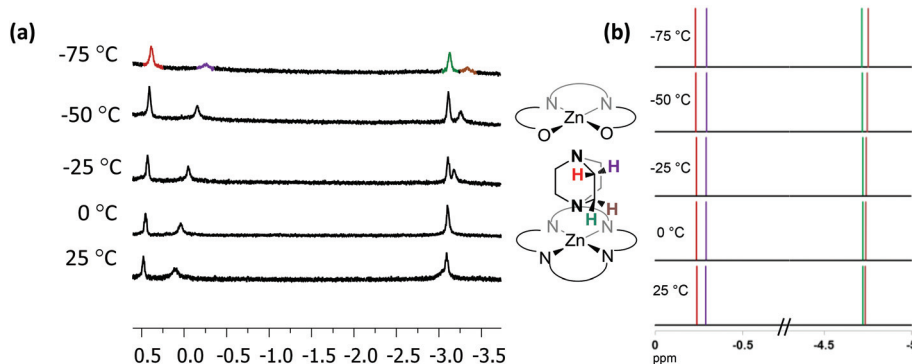


Fig. 3 Partial VT ^1H NMR (600 MHz) of ROT-2 in CD_2Cl_2 at various temperatures. (a) Experimental and (b) computed spectra.

H^2 and H^3 will appear as average values; the same is true for H^a , H^b and H^c . The averaging was applied for both **Conf-1_M** and **Conf-2_M** separately. Finally, Boltzmann weightage was applied at various temperatures and the computed NMR spectra are represented in Fig. 3b. Computed NMRs deviate only a little with respect to the experiment. The shifts of the downfield signals near -0.2 ppm are less pronounced in the computations but they are in line with the experiment. Computed upfield signals near -4.7 ppm clearly separate on lowering the temperature. By considering the size of the system and the approximation made to compute the NMR, the match of the computed NMR with the experimental one is qualitatively excellent. From the variable temperature experiment and computational analysis, it is evident that the DABCO residue in **ROT-2** rotates rapidly while being sandwiched in between salphen and porphyrin. Further splitting of the DABCO signals on lowering the temperature is a result of changing populations of different conformers, namely **Conf-1** and **Conf-2**.

Conclusion

In conclusion, we prepared and characterised the new salphen ligand **2** and incorporated it into the four-component nanorotor **ROT-2**. The rotational rate in **ROT-2** was found to be much lower than that of **ROT-3**, a previously described system.^{18a} Computations demonstrated that **ROT-2'** has a much higher ground-state stabilisation than **ROT-3'**; the difference amounts to 33.9 kJ mol⁻¹. Interestingly, the experimental rotational barrier of **ROT-2** is higher than that of **ROT-3** by the same token, *i.e.* 32.0 kJ mol⁻¹. Such a finding suggests that the high ground-state stabilisation of **ROT-2** leads to a very slow rotation. In addition, the geminal hydrogens in DABCO are diastereotopic in **ROT-2**. As the experimental and computed proton shifts, both at low and high temperatures, agree rather well, it is clear that the DABCO is sandwiched between the zinc porphyrin and zinc salphen moieties, despite some contradictory evidence from the ESI mass spectral analysis.

Experimental part

General remarks

¹H and ¹³C NMR spectra were recorded on Bruker Avance (400 MHz) and Varian (600 MHz) spectrometers using a deuterated solvent as the lock and a residual protiated solvent as the internal reference. The following abbreviations were utilised to describe the signal patterns: s = singlet, d = doublet, t = triplet, dd = doublet of doublets, td = triplet of doublets, dt = doublet of triplets, br = broad and m = multiplet. Electrospray ionisation (ESI) mass spectra were recorded on a Thermo-Quest LCQ deca. The melting points were measured on a Büchi SMP-20 and are uncorrected. Infrared spectra were recorded on a Varian 1000 FT-IR instrument. Elemental analysis was done using the EA 3000 CHNS. Commercial reagents were

used without further purification. Et₃N was distilled over calcium hydride. A general outline for the preparation of rotator **2** is provided in Scheme 1. 2-Hydroxy-3-*tert*-butyl-benzaldehyde (**5**),²³ 5-bromo-3-*tert*-butyl-2-hydroxybenzaldehyde (**6**),²⁴ 3-(*tert*-butyl)-2-hydroxy-5-(4,4,5,5-tetramethyl-1,3,2-dioxaborolan-2-yl)benzaldehyde (**7**),²⁵ 1,4-dibromo-2,3,5,6-tetramethylbenzene (**8**)²⁶ and stator **1**^{18a} were synthesised according to the literature methods. The numbering of the carbon skeleton in the molecular formulae as shown in the manuscript does not comply with the IUPAC nomenclature rules; it is only used for assignments of NMR signals. The ROESY spectrum was obtained with a 1.5 s relaxation delay, using 2 K data points in the t_2 dimension and 400 in t_1 . Scans were taken for each measurement (32 scans) and the spectrum was recorded with 300 ms mixing time.

4'-Bromo-5-*tert*-butyl-4-hydroxy-2',3',5',6'-tetramethylbiphenyl-3-carbaldehyde (9). A modified literature procedure was followed.²⁶ A Schlenk tube charged with 3-*tert*-butyl-2-hydroxy-5-(4,4,5,5-tetramethyl-1,3,2-dioxaborolan-2-yl)benzaldehyde (**7**) (500 mg, 1.64 mmol), 1,4-dibromo-2,3,5,6-tetramethylbenzene (**8**) (572 mg, 1.97 mmol), Pd(PPh₃)₄ (95 mg, 0.082 mmol) and K₂CO₃ (340 mg, 2.46 mmol) was placed under N₂ by successive vacuum-N₂ cycles. Thoroughly degassed DME (6 mL) and degassed water (1.2 mL) were introduced *via* a cannula into the Schlenk vessel. The mixture was heated at 90 °C for 24 h. Water (20 mL) was added and the aqueous layer was extracted with CH₂Cl₂ (3 × 50 mL). The organic layer was dried over MgSO₄ and the solvents were removed under reduced pressure. The residue was purified by a column on silica gel (hexane/ethyl acetate = 99 : 1, R_f = 0.26) to afford the expected product (353 mg, 55%) as a white solid; mp: 126 °C; ¹H NMR (400 MHz, CDCl₃) δ 11.81 (s, 1H, OH), 9.87 (d, J = 4.6 Hz, 1H, CHO), 7.26 (d, J = 2.1 Hz, 1H, H_{ar}), 7.12 (d, J = 2.1 Hz, 1H, H_{ar}), 2.47 (s, 6H, CH₃), 2.00 (s, 6H, CH₃), 1.43 (s, 9H, *t*Bu); ¹³C NMR (101 MHz, CDCl₃) δ 197.3, 160.1, 140.0, 138.8, 135.6, 134.2, 133.9, 133.0, 132.1, 128.8, 120.6, 35.1, 29.5, 21.4, 19.4; IR (KBr) ν 2998, 2959, 2865, 1639, 1411, 1382, 1360, 1267, 1225, 1172, 778, 699 cm⁻¹; Anal. Calcd for C₂₁H₂₅BrO₂: C, 64.78; H, 6.47; found: C, 64.63; H, 6.37.

5-*tert*-Butyl-4-hydroxy-2',3',5',6'-tetramethyl-4'-(pyridin-4-yl)biphenyl-3-carbaldehyde (10). A mixture of aldehyde **9** (250 mg, 642 μ mol), 4-pyridinyl boronic acid (87 mg, 0.71 mmol), sodium carbonate (102 mg, 962 μ mol) and Pd(dppf)Cl₂ (26.0 mg, 35.5 μ mol) was stirred in DME : H₂O (v/v 3 : 1, 8 mL, degassed with N₂) and stirred at 100 °C for 3 h. After cooling to rt, the reaction contents were poured into H₂O (10 mL). The aqueous mixture was extracted with CH₂Cl₂ (3 × 15 mL) and the combined extracts were dried over MgSO₄ before being concentrated under reduced pressure. The crude aldehyde was purified by flash chromatography on silica gel (DCM/EtOAc = 4 : 1, R_f = 0.33) to afford a white solid (238 mg, 96%); mp: 155 °C; ¹H NMR (400 MHz, CDCl₃) δ 11.81 (s, 1H, OH), 9.88 (s, 1H, CHO), 8.70 (br d, J = 4.7 Hz, 2H, [α and α']-H), 7.35 (d, J = 2.1 Hz, 1H, H_{ar}), 7.20 (d, J = 2.1 Hz, 1H, H_{ar}), 7.16 (br d, J = 4.7 Hz, 1H, [β or β']-H), 7.15 (br d, J = 4.7 Hz, 1H, [β' or β]-H), 1.98 (s, 6H, CH₃), 1.95 (s, 6H, CH₃), 1.45 (s, 9H,

*t*Bu); ^{13}C NMR (101 MHz, CDCl_3) δ 197.3, 160.1, 151.2, 150.1, 140.8, 139.0, 138.7, 135.7, 133.2, 132.8, 132.2, 131.3, 125.0, 120.7, 35.2, 29.5, 18.3, 18.2; IR (KBr) ν 2923, 2853, 1651, 1594, 1448, 1407, 1265, 1265, 1201, 1162, 812, 738, 770 cm^{-1} ; Anal. Calcd for $\text{C}_{26}\text{H}_{29}\text{NO}_2$: C, 80.59; H, 7.54; N, 3.61; found: C, 80.66; H, 7.60; N, 3.47.

Synthesis of salphen ligand 2. Following a general procedure,^{20a} a solution of 4,5-dimethyl-1,2-phenylenediamine (16.7 mg, 0.120 mmol), aldehyde 10 (100 mg, 0.260 mmol), $\text{Zn}(\text{OAc})_2 \cdot 2\text{H}_2\text{O}$ (81.0 mg, 0.370 mmol) and neat NEt_3 (100 μL) in MeOH (6 mL) was stirred for 18 h at room temperature. The desired compound was isolated by filtration and dried *in vacuo* to yield an orange solid (99 mg, 86%); mp: 117 $^\circ\text{C}$; ^1H NMR (400 MHz, DMSO) δ 9.01 (s, 2H, e-H), 8.67 (d, $J = 5.2$ Hz, 4H, d-H), 7.70 (s, 2H, f-H), 7.23 (d, $J = 5.2$ Hz, 4H, c-H), 7.06 (d, $J = 2.1$ Hz, 2H, H_{ar}), 6.96 (d, $J = 2.1$ Hz, 2H, H_{ar}), 2.32 (s, 6H, CH_3), 2.02 (s, 12H, CH_3), 1.88 (s, 12H, CH_3), 1.52 (s, 18H, *t*Bu); ^{13}C NMR (101 MHz, DMSO) δ 170.5, 161.5, 150.5, 149.8, 142.0, 141.4, 137.7, 137.1, 135.5, 133.9, 132.2, 131.6, 130.1, 124.9, 119.1, 116.7, 35.2, 29.7, 19.6, 18.1, 17.9; IR (KBr) ν 2923, 2853, 1612, 1589, 1519, 1463, 1382, 1219, 1158, 1021, 815, 793, 488 cm^{-1} ; ESI-MS: m/z (%) 937 (100) $[\text{M} + \text{H}]^+$ Anal. Calcd for $\text{C}_{60}\text{H}_{64}\text{N}_4\text{O}_2\text{Zn} \cdot 2\text{H}_2\text{O}$: C, 73.94; H, 7.03; N, 5.75; found: C, 74.16; H, 6.93; N, 5.42.

Preparation of ROT-1. In an NMR tube stator 1 (2.01 mg, 0.808 μmol), rotator 2 (0.758 mg, 0.808 μmol) and DABCO (91.0 μg , 0.808 μmol) were mixed in CD_2Cl_2 . Then, after the addition of $[\text{Cu}(\text{CH}_3\text{CN})_4]\text{PF}_6$ (602 μg , 1.62 μmol) the solution was sonicated for 1 h to afford ROT-1; mp: 150 $^\circ\text{C}$; ^1H NMR (400 MHz, CD_2Cl_2): δ 8.99 (d, $J = 4.6$ Hz, 2H, β -H), 8.97 (d, $J = 4.6$ Hz, 2H, β -H), 8.94 (d, $J = 4.6$ Hz, 2H, β -H), 8.90 (d, $J = 4.6$ Hz, 2H, β -H), 8.81 (d, $J = 8.1$ Hz, 2H, [4 or 7]-H, complexed), 8.79 (d, $J = 8.1$ Hz, 2H, [4 or 7]-H, complexed), 8.46 (br s, 4H, [10 or 11]-H), 8.40 (d, $J = 8.1$ Hz, 2H, [4 or 7]-H, uncomplexed), 8.37 (d, $J = 8.1$ Hz, 2H, [4 or 7]-H, uncomplexed), 8.36 (br s, 2H, [10 or 11]-H), 8.26 (s, 4H, [5 and 6]-H, complexed), 8.24 (br d, $J = 8.2$ Hz, 1H, [10 or 11]-H), 8.10 (br d, $J = 8.2$ Hz, 1H, [10 or 11]-H), 8.07 (d, $J = 8.1$ Hz, 2H, [3 or 8]-H, complexed), 8.04 (s, 4H, [10 or 11]-H), 8.02 (d, $J = 8.1$ Hz, 2H, [3 or 8]-H, complexed), 7.97 (br d, $J = 8.2$ Hz, 1H, [10 or 11]-H), 7.95 (br d, $J = 8.2$ Hz, 1H, [10 or 11]-H), 7.94 (s, 4H, [5 and 6]-H, uncomplexed), 7.89 (br d, $J = 8.2$ Hz, 1H, [10 or 11]-H), 7.81 (br d, $J = 8.2$ Hz, 1H, [10 or 11]-H), 7.60 (d, $J = 8.1$ Hz, 2H, [3 or 8]-H, uncomplexed), 7.59 (d, $J = 8.1$ Hz, 2H, [3 or 8]-H, uncomplexed), 7.19 (br s, 2H, e-H), 7.07 (br s, 4H, 9-H, complexed), 7.01 (br d, $J = 5.0$ Hz, 4H, c-H), 6.99 (s, 4H, 9-H, uncomplexed), 6.92 (br d, $J = 5.0$ Hz, 4H, d-H), 6.91 (s, 2H, f-H), 6.81 (br s, 2H, [b or a]-H), 6.55 (br d, $J = 1.8$ Hz, 2H, [a or b]-H), 2.71 (s, 12H, CH_3), 2.69 (s, 12H, CH_3), 2.51 (s, 6H, CH_3), 2.36 (s, 12H, CH_3), 2.34 (s, 12H, CH_3), 2.23 (s, 6H, CH_3), 2.17 (s, 6H, CH_3), 2.15 (s, 12H, CH_3), 2.07 (s, 12H, CH_3), 2.05 (s, 12H, CH_3), 2.02 (s, 12H, CH_3), 1.21 (s, 18H, *t*-Bu), 0.47 (br t, $J = 7.4$ Hz, 6H, DABCO), -3.10 (br t, $J = 7.7$ Hz, 6H, DABCO); IR (KBr) ν 2922, 2852, 1613, 1587, 1494, 1460, 1382, 1357, 1161, 996, 841, 557 cm^{-1} ; Anal. Calcd for $\text{C}_{242}\text{H}_{216}\text{Cu}_4\text{F}_{24}\text{N}_{18}\text{O}_2\text{P}_2\text{Zn}_2 \cdot 5\text{CH}_2\text{Cl}_2$: C, 67.72; H, 5.20; N, 5.75; found: C, 67.62; H, 4.96; N, 5.52.

Preparation of ROT-2. $[\text{Cu}(\text{CH}_3\text{CN})_4]\text{PF}_6$ (602 μg , 1.62 μmol) in CD_2Cl_2 was added to ROT-1 (in an NMR tube) and the mixture was sonicated for 15 min to furnish ROT-2; mp: 151 $^\circ\text{C}$; ^1H NMR (400 MHz, CD_2Cl_2): δ 9.05 (br s, 2H, β -H), 8.99 (d, $J = 4.6$ Hz, 2H, β -H), 8.95 (d, $J = 4.6$ Hz, 1H, β -H), 8.94 (d, $J = 4.6$ Hz, 1H, β -H), 8.90 (d, $J = 4.6$ Hz, 2H, β -H), 8.81 (d, $J = 8.5$ Hz, 2H, [4 or 7]-H, complexed), 8.78 (d, $J = 8.5$ Hz, 2H, [4 or 7]-H, complexed), 8.74 (d, $J = 8.5$ Hz, 1H, [4 or 7]-H, Cu^+ loaded), 8.73 (d, $J = 8.5$ Hz, 1H, [4 or 7]-H, Cu^+ loaded), 8.70 (d, $J = 8.5$ Hz, 1H, [4 or 7]-H, Cu^+ loaded), 8.69 (d, $J = 8.5$ Hz, 1H, [4 or 7]-H, Cu^+ loaded), 8.47 (br s, 2H, [10 or 11]-H), 8.46 (br d, $J = 7.7$ Hz, 1H, [10 or 11]-H), 8.39 (br d, $J = 7.7$ Hz, 1H, [10 or 11]-H), 8.32 (br d, $J = 7.7$ Hz, 1H, [10 or 11]-H), 8.25 (s, 6H, [5 and 6]-H, complexed and [10 or 11]-H), 8.18 (s, 6H, [5 and 6]-H, Cu^+ loaded and [10 or 11]-H), 8.09–8.00 (m, 7H, [3 and 8]-H, complexed and [10 or 11]-H), 8.00–7.91 (m, 6H, [3 and 8]-H, Cu^+ loaded and [10 or 11]-H), 7.89 (br d, $J = 7.7$ Hz, 1H, [10 or 11]-H), 7.83 (br d, $J = 7.7$ Hz, 1H, [10 or 11]-H), 7.19 (br s, 2H, e-H), 7.07 (br s, 4H, 9-H, complexed), 7.05 (s, 4H, 9-H, Cu^+ loaded), 7.01 (br d, $J = 5.4$ Hz, 4H, c-H), 6.94 (d, $J = 5.4$ Hz, 4H, d-H), 6.91 (br s, 2H, f-H), 6.81 (br d, $J = 1.6$ Hz, 2H, [b or a]-H), 6.56 (br d, $J = 1.6$ Hz, 2H, [a or b]-H), 2.72 (s, 12H, CH_3), 2.71 (s, 6H, CH_3), 2.70 (s, 6H, CH_3), 2.51 (s, 6H, CH_3), 2.38 (s, 12H, CH_3), 2.33 (s, 12H, CH_3), 2.23 (s, 6H, CH_3), 2.17 (s, 6H, CH_3), 2.15 (s, 12H, CH_3), 2.06 (s, 12H, CH_3), 2.05 (s, 12H, CH_3), 2.02 (s, 12H, CH_3), 1.21 (s, 18H, *t*-Bu), 0.47 (br t, $J = 7.6$ Hz, 3H, CH_2 -DABCO), 0.11 (br s, 3H, CH_2 -DABCO) -3.10 (br t, $J = 7.6$ Hz, 6H, CH_2 -DABCO); IR (KBr) ν 2922, 2853, 1612, 1586, 1494, 1459, 1383, 1356, 1166, 996, 841, 557 cm^{-1} ; Anal. Calcd for $\text{C}_{242}\text{H}_{216}\text{Cu}_4\text{F}_{24}\text{N}_{18}\text{O}_2\text{P}_4\text{Zn}_2 \cdot 3\text{CH}_2\text{Cl}_2$: C, 63.58; H, 4.83; N, 5.45; found: C, 63.31; H, 4.61; N, 5.49.

Acknowledgements

We thank the DFG (Schm 647/20-1) and the University of Siegen for their continued support in particular for providing the Linux Cluster HorUS for computations.

References

- 1 V. Richards, *Nat. Chem.*, 2016, **8**, 1090.
- 2 M. A. Watson and S. L. Cockroft, *Chem. Soc. Rev.*, 2016, **45**, 6118–6129.
- 3 V. Balzani, A. Credi and M. Venturi, *Chem. Soc. Rev.*, 2009, **38**, 1542–1550.
- 4 (a) S. Erbas-Cakmak, D. A. Leigh, C. T. McTernan and A. L. Nussbaumer, *Chem. Rev.*, 2015, **115**, 1008–10206; (b) E. R. Kay and D. A. Leigh, *Angew. Chem., Int. Ed.*, 2015, **54**, 10080–10088.
- 5 S. De, K. Mahata and M. Schmittle, *Chem. Soc. Rev.*, 2010, **39**, 1555–1575.
- 6 K. Mahata and M. Schmittle, *J. Am. Chem. Soc.*, 2009, **131**, 16544–16554.

- 7 K. Mahata, M. Lal Saha and M. Schmittel, *J. Am. Chem. Soc.*, 2010, **132**, 15933–15935.
- 8 D. M. Wood, W. Meng, T. K. Ronson, A. R. Stefankiewicz, J. K. M. Sanders and J. R. Nitschke, *Angew. Chem., Int. Ed.*, 2015, **54**, 3988–3992.
- 9 W. M. Bloch, Y. Abe, J. J. Holstein, C. M. Wandtke, B. Dittrich and G. H. Clever, *J. Am. Chem. Soc.*, 2016, **138**, 13750–13755.
- 10 D. Preston, J. E. Barnsley, K. C. Gordon and J. D. Crowley, *J. Am. Chem. Soc.*, 2016, **138**, 10578–10585.
- 11 (a) M. von Delius, E. M. Geertsema and D. A. Leigh, *Nat. Chem.*, 2010, **2**, 96; (b) D. A. Leigh, U. Lewandowska, B. Lewandowski and M. R. Wilson, *Top. Curr. Chem.*, 2014, **354**, 111.
- 12 (a) A. Credi, S. Silvi and M. Venturi, *Top. Curr. Chem.*, 2014, **354**, 1; (b) C. J. Bruns and J. F. Stoddart, *Acc. Chem. Res.*, 2014, **47**, 2186.
- 13 G. S. Kottas, L. I. Clarke, D. Horinek and J. Michl, *Chem. Rev.*, 2005, **105**, 1281–1376.
- 14 R. Hernandez, H.-R. Tseng, J. W. Wong, J. F. Stoddart and J. I. Zink, *J. Am. Chem. Soc.*, 2004, **126**, 3370–3371.
- 15 S. Silvi, A. Arduini, A. Pochini, A. Secchi, M. Tomasulo, F. M. Raymo, M. Baroncini and A. Credi, *J. Am. Chem. Soc.*, 2007, **129**, 13378–13379.
- 16 S. Hiraoka, E. Okuno, T. Tanaka, M. Shiro and M. Shionoya, *J. Am. Chem. Soc.*, 2008, **130**, 9089–9098.
- 17 S. Hiraoka, Y. Hisanaga, M. Shiro and M. Shionoya, *Angew. Chem., Int. Ed.*, 2010, **49**, 1669–1673.
- 18 (a) S. K. Samanta and M. Schmittel, *J. Am. Chem. Soc.*, 2013, **135**, 18794–18797; (b) S. K. Samanta, J. W. Bats and M. Schmittel, *Chem. Commun.*, 2014, **50**, 2364–2366; (c) S. K. Samanta, A. Rana and M. Schmittel, *Angew. Chem., Int. Ed.*, 2016, **55**, 2267–2272.
- 19 (a) M. Schmittel, B. He, J. Fan, J. W. Bats, M. Engeser, M. Schlosser and H.-J. Deiseroth, *Inorg. Chem.*, 2009, **48**, 8192–8200; (b) S. Neogi, G. Schnakenburg, Y. Lorenz, M. Engeser and M. Schmittel, *Inorg. Chem.*, 2012, **51**, 10832–10841.
- 20 (a) A. W. Kleij, M. Kuil, D. M. Tooke, M. Lutz, A. L. Spek and J. N. H. Reek, *Chem. – Eur. J.*, 2005, **11**, 4743–4750; (b) A. W. Kleij, M. Kuil, M. Lutz, D. M. Tooke, A. L. Spek, P. C. J. Kamer, P. W. N. M. van Leeuwen and J. N. H. Reek, *Inorg. Chim. Acta*, 2006, **359**, 1807–1814.
- 21 S. J. Wezenberg and A. W. Kleij, *Angew. Chem., Int. Ed.*, 2008, **47**, 2354–2364.
- 22 B. Doistau, A. Tron, S. A. Denisov, G. Jonusauskas, N. D. McClenaghan, G. Gontard, V. Marvaud, B. Hasenknopf and G. Vives, *Chem. – Eur. J.*, 2014, **20**, 15799–15807.
- 23 U. Streit, F. Birbaum, A. Quattropani and C. G. Bochet, *J. Org. Chem.*, 2013, **78**, 6890–6910.
- 24 W.-S. Kim, K. Y. Lee, E.-H. Ryu, J.-M. Gu, Y. Kim, S. J. Lee and S. Huh, *Eur. J. Inorg. Chem.*, 2013, 4228–4233.
- 25 F. Ibrahim, H. Nasrallah, X. Hong, M. Mellah, A. Hachem, G. Ibrahim, N. Jaber and E. Schulz, *Tetrahedron*, 2012, **68**, 9954–9961.
- 26 I. Kaur, M. Jazdyk, N. N. Stein, P. Prusevich and G. P. Miller, *J. Am. Chem. Soc.*, 2010, **132**, 1261–1263.
- 27 S. J. Wezenberg, E. C. Escudero-Adán, J. Benet-Buchholz and A. W. Kleij, *Org. Lett.*, 2008, **10**, 3311–3314.
- 28 (a) C. A. Hunter, M. N. Meah and J. K. M. Sanders, *J. Am. Chem. Soc.*, 1990, **112**, 5773–5780; (b) S. K. Samanta, D. Samanta, J. W. Bats and M. Schmittel, *J. Org. Chem.*, 2011, **76**, 7466–7473.
- 29 S. Liu, D. V. Kondratuk, S. A. L. Rousseaux, G. Gil-Ramírez, M. C. O'Sullivan, J. Cremers, T. D. W. Claridge and H. L. Anderson, *Angew. Chem., Int. Ed.*, 2015, **127**, 5445–5449.
- 30 H. Günther, *NMR Spectroscopy: Basic Principles, Concepts and Applications in Chemistry*, Wiley-VHC, Weinheim, 3rd edn, 2013, ch. 13, pp. 501–556.
- 31 M. J. Frisch, *et al.*, *Gaussian 09, Rev. D.01*, Gaussian, Inc., Wallingford, CT, 2009.
- 32 The B3LYP functional in combination with Grimme's D3 dispersion was considered for optimisation. All the nitrogen atoms in the high layer was treated with the 6-31+G* basis set and other main group elements were by 3-21G. For copper LANL2DZ effective core potential (ECP) was used for the core electrons. The valence electrons were treated with the LANL2DZ basis set.
- 33 N. C. Burtch, A. Torres-Knoop, G. S. Foo, J. Leisen, C. Sievers, B. Ensing, D. Dubbeldam and K. S. Walton, *J. Phys. Chem. Lett.*, 2015, **6**, 812–816.
- 34 For the DFT method B3LYP functional combined with Grimme's D3 dispersion was chosen. The 6-31G* basis set was used for all the main group elements and for zinc the LANL2DZ basis set was used for valence electrons, the core electrons were replaced by LANL2DZ ECP.
- 35 Computed at the GIAO-B3LYP/6-31+G**/PCM(CH₂Cl₂) level.